Article ID: 1006-8775(2020) 04-0402-15

The Effect of Warm Water and Its Weak Negative Feedback on the Rapid Intensification of Typhoon Hato (2017)

HUO Zi-mo (霍子墨), DUAN Yi-hong (端义宏), LIU Xin (刘 欣)
(State Key Laboratory of Severe Weather, Chinese Academy of Meteorological Sciences, Beijing 100081 China)

Abstract: Typhoon Hato (2017) went through a rapid intensification (RI) process before making landfall in Zhuhai, Guangdong Province, as the observational data shows. Within 24 hours, its minimum sea level pressure deepened by 35hPa and its maximum sustained wind speed increased by 20m s^{-1}. According to satellite observations, Hato encountered a large area of warm water and two warm core rings before the RI process, and the average sea surface temperature cooling (SSTC) induced by Hato was only around 0.73℃. Air-sea coupled simulations were implemented to investigate the specific impact of the warm water on its RI process. The results showed that the warm water played an important role by facilitating the RI process by around 20%. Sea surface temperature budget analysis showed that the SSTC induced by mixing mechanism was not obvious due to the warm water. Besides, the cold advection hardly caused any SSTC, either. Therefore, the SSTC induced by Hato was much weaker compared with that in general cases. The negative feedback between ocean and Hato was restrained and abundant heat and moisture were sufficiently supplied to Hato. The warm water helped heat flux increase by around 20%, too. Therefore, the warm water influenced the structure and the intensity of Hato. Although there might be other factors that also participated in the RI process, this study focused on air-sea interaction in tropical cyclone forecast and discussed the impact of warm water on the intensity and structure of a tropical cyclone.

Key words: Typhoon Hato; rapid intensification; warm water; air-sea coupled model; sea surface temperature cooling
CLC number: P444 **Document code:** A
https: //doi.org/10.46267/j.1006-8775.2020.035

1 INTRODUCTION

Among the typhoons that made landfall in China in 2017, Hato was the strongest one (Wang et al. [1]). It caused severe casualties and property damage in Guangdong, Hong Kong and Macau due to its strong intensity. According to the best track data provided by the China Meteorological Administration (CMA), Hato went through a rapid intensification (RI) process in the nearshore region and posed a critical challenge to its forecast.

The intensity change of tropical cyclones (TCs) is always a complicated topic as a lot of factors are involved (Elsberry et al. [2]). Previous researches showed that critical factors include the intrinsic inner structure of TC itself, the environmental field and the underlying surface (Merrill [3]; Emanuel [4]; Kaplan and DeMaria [5]; Wang and Wu [6]; Duan et al. [7]). Studies show that among all the elements the interaction between air and sea plays quite a vital role in the development of TCs (Emanuel [8]), as TCs all generate and spend most of their lifetime moving on oceans. In early years, ocean was simply seen as the energy source of TCs. Many researchers believed that high sea surface temperature (SST) would benefit the development of TCs (Palmén [9]; Miller [10]). Emanuel put forward a theory in which a TC is basically a Carnot heat engine [11]. He found the maximum potential intensity (MPI) of a TC increases with the SST underneath. Despite the obvious deficiencies in the MPI theory, it cannot be denied that high SST is a very important factor for TC development. Xu et al. found that SST not only influences the MPI, but also influences the intensification rate of a TC [12]. SST directly influences the exchange of heat and moisture at the interface of ocean and atmosphere (Cione and Uhlhorn [13]; Zheng et al. [14]; Wang et al. [15]; Wang et al. [16]), and around 1℃ of SST change in the inner-core region of a TC can result in the total enthalpy flux change by 40% (Cione and Uhlhorn [13]). Ye et al. found that TC intensity is highly sensitive to the latent heat in the inner-core region [16]. This is the positive feedback between ocean and TCs.

There is also a negative feedback between ocean and TCs that cannot be neglected: the intensification of

Received 2020-02-25 **Revised** 2020-08-15 **Accepted** 2020-11-15
Funding: National Basic R&D Project (973 Program) of China (2015CB452805); National Natural Science Foundation of China (61827901); National Key R&D Program of China (2017YFC1501602); Open Research Program of the State Key Laboratory of Severe Weather (2019LASW-A08); Basic Research Fund of CAMS (2016Z003, 2018Y013); Program of the National Satellite Meteorological Centre (FY3(02P)-MAS-1803)
Biography: HUO Zi-mo, M.S., primarily undertaking research on tropical cyclones.
Corresponding author: DUAN Yi-hong, Ph. D., e-mail: duanyh@cma.gov.cn

TC can be held back by the TC-induced SST cooling (SSTC) (Chang and Anthes [17]). It's widely observed and computationally verified that TCs can induce SSTC, especially on the right side of TC tracks (Leipper [18]; Price [19]; Chu et al. [20]; Jacob et al. [21]; Lin et al. [22]; Sanford et al. [23]; Potter et al. [24]). SSTC occurs under the effect of the wind stress of the TC bottom layer on the sea surface. Vertical turbulent mixing and advection are the two main mechanisms of SSTC. Price gave a specific explanation of the phenomenon of SSTC [19]. First, the wind stress imposed on the ocean surface generates ocean currents. The upper layer water flows faster while the deeper layer water flows rather slowly, which would result in vertical shear of ocean currents. Then the vertical current shear results in vertical turbulent mixing and entrainment. Besides, under the influence of the Ekman pumping caused by the cyclonic circulation of TCs, the deep-layer cold water is pumped above, which is an important form of vertical advection. In addition, the direct heat and moisture exchange between air and sea also takes part in SSTC, though very limited in extent. Generally, the SSTC induced by TC is about 1℃ to 6℃. Price illustrated the rightward bias of SSTC as well. Because the turning direction of the wind stress on the right side resonates with the ocean currents of the mixing layer, stronger entrainment occurs[19]. Moreover, Ginis came up with another idea that there are inertially rotating currents that would cause divergent variation of water [25]. On the right of the track, the divergence of ocean current velocity is positive, and that will shallow the mixing layer. Therefore, SSTC becomes stronger.

SSTC could inhibit the transfer of heat and moisture so it is an important factor retarding TC development. This negative feedback is verified by many researchers using numerical models (Schade and Emanuel [26]; Chan et al. [27]; Davis et al. [28]; Zeng and Chen [29]; Duan et al. [30]; Li et al. [31]; Zhao and Chan [32]; Liu et al. [33]; Liu et al. [34]). In fact, the negative feedback is found closely connected to various parameters like movement speed, MPI, horizontal size of the storm, depth of ocean mixing layer and the thermal stratification below (Schade and Emanuel [26]; Zeng and Chen [29]; Zhao and Chan [32]).

Therefore, it is necessary to pay attention to the interaction between ocean and Hato when studying its RI process. It is notable that Hato encountered some meso-scale warm water features when it moved on the ocean, as is depicted in Fig. 1. It shows the sea level anomaly (SLA) pattern around the track of Hato on August 19, 2017, the time when it generated. SLA is defined as the difference between the instantaneous sea surface height (SSH) and the climatologically mean SSH (here it refers to the 1993–2012 period), which is often used to recognize meso-scale features in the ocean, instead of SST. That is because SLA is mostly a manifestation of the overall warming of the vertical water column, which can hardly be recognized through an isolated layer of temperature distribution. As can be seen, before Hato came to the South China Sea, it moved over a large area of warm water; after that, it encountered two warm core rings (WCRs) in the Luzon Strait and in the South China Sea successively. According to the best track data provided by the CMA, Hato intensified rapidly right after interacting with warm water.

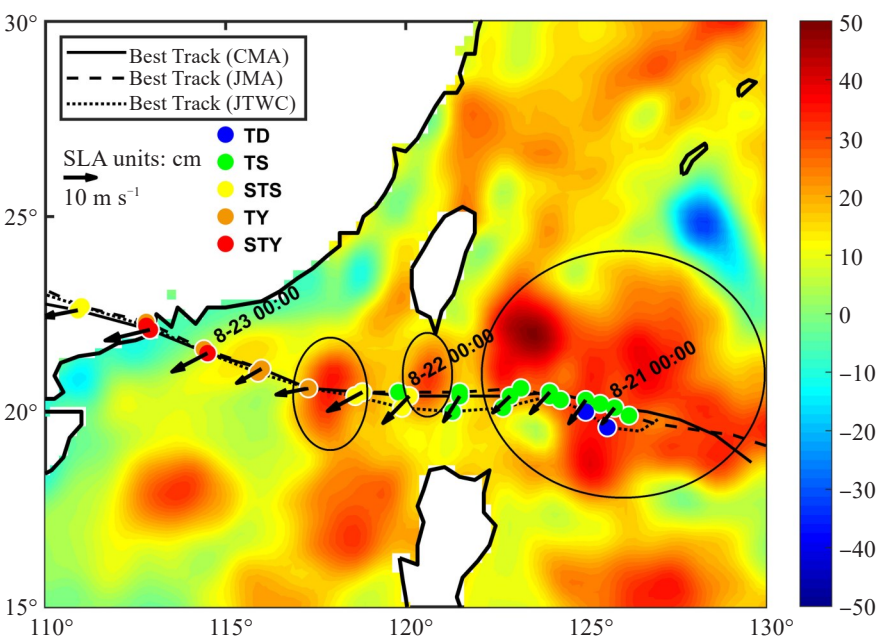

Figure 1. The distribution of SLA on August 19, 2017. The three black lines (solid, dashed and dotted) represent the best tracks of Hato from CMA, JMA, and JTWC, and the colorful dots stand for its intensity category according to CMA standards. The black arrows sticking out from the CMA best track are the vertical wind shear between 850hPa and 200hPa along its trajectory. The three big circles highlight the three high value zones of SLA.

Many studies show that meso-scale features in the ocean such as WCRs and western boundary current could have impact on TCs by changing local ocean subsurface conditions (Hong et al. [35]; Shay et al. [36]; Lin et al. [37]; Lin et al. [38]; Kuo et al. [39]; Wang et al. [40]). Similarly, Hurricane Opal (1995) encountered a WCR in the Gulf of Mexico then went through a RI process. Hong et al. [35] and Shay et al. [36] both conducted studies on this phenomenon. Their results indicated that around 60% of the intensification after Opal moving over the WCR was contributed by it, and Opal extracted around 40% of the available heat capacity from the WCR, indicating that the WCR was a major factor of the RI process of Opal. Wang et al. found that it was the WCR and the SST warming caused by climate change that jointly led to the RI process of Super Typhoon Haiyan (2013), while the WCR imposed a more obvious influence [40]. Lin et al. categorized all the 30 category-5 TCs in the northwest Pacific Ocean from 1993 to 2005 [38]. They found TCs in the south eddy zone and the Kuroshio region, where the climatological warm layer of ocean was shallow, were distinctly affected by warm water as they deepened the warm layer.

It is reasonable to assume that warm water had significant impact on Hato's RI process. There are other researchers that have conducted some studies on RI process (Zhang et al. [41]; Qin et al. [42]). They all agreed that apart from the appropriate atmospheric condition, the high SST possibly contributed to the RI of Hato. Therefore, the main aim of the study is to understand how and to what extent did warm water influence the RI of Hato. In our study, an air-sea coupled model is used to analyze these questions.

Data, models and experimental design are introduced in section 2. The observation of SLA and Hato, the simulation results and their comparison are presented in section 3. The outcomes are discussed in section 4 and conclusions are given in section 5.

2 DATA, MODELS AND EXPERIMENTAL DESIGN

2.1 *Data*

TC best track data provided by three different agencies including CMA (http://tcdata.typhoon.org.cn/) (Ying et al. [43]), Japan Meteorological Agency (JMA, http://www.jma.go.jp/jma/jma-eng/jma-center/rsmc-hp-pub-eg/trackarchives.html) and Joint Typhoon Warning Center (JTWC, https://www.metoc.navy.mil/jtwc/jtwc.html?best-tracks) are used and compared in our study. All of them have 6-hourly TC information; however, CMA and JTWC would have some 3-hourly records when TCs are in the nearshore region. In addition, the movement speed of Hato is calculated with the TC information provided by the National Meteorological Center of CMA. It derives from the operational observation and has hourly TC records which would help calculate more precisely. Radar base data from Guangzhou Radar Station is used to compare the structure of Hato.

SST and SSH data are used to analyze the marine environment. SST data used here is the Advanced Very High Resolution Radiometer SST product (AVHRR-only), also known as OISST. It is from the National Oceanic and Atmospheric Administration (NOAA, https://www.ncdc.noaa.gov/oisst) and it is daily, 0.25°×0.25° gird data. SLA daily data is obtained from Archiving, Validation, and Interpretation of Satellite Oceanographic data (AVISO, http://www.aviso.oceanobs.com) with a resolution of 0.25°×0.25°.

Besides, Simple Ocean Data Assimilation data (SODA, http://dsrs.atmos.umd.edu/, Carton et al. [44]; Carton et al. [45]) is used for the initial and boundary fields for the ocean model, which contains ocean currents, SST, SSH and plenty of other ocean variables with a 5-day temporal resolution and a 0.5°×0.5° spatial resolution. The NCEP Final (FNL) Operational Global Analysis data (https://rda.ucar.edu/datasets/ds083.3/) is utilized in the atmospheric model as the initial and boundary fields, and it's daily and 0.25°×0.25°.

2.2 *Models*

The interaction between air and sea is the main focus of the study. Therefore, the Coupled-Ocean-Atmosphere-Wave-Sediment Transport (COAWST, https://woodshole.er.usgs.gov/project-pages/cccp/public/COAWST.htm) Modeling system is adopted here (Warner et al. [46]).

COAWST model combines Regional Ocean Modeling System version 3.7 (ROMS, https://www.myroms.org/) and Weather Research and Forecasting Model - the Advanced Research WRF version 3.9.1.1 (WRF-ARW, https://www.mmm.ucar.edu/weather-research-and-forecasting-model). WRF-ARW is a quasi-compressible, non-hydrostatic atmospheric model and it is one of the most commonly used models in typhoon research. ROMS is a 3-D, free-surface, terrain-following ocean model. Variables in different components are exchanged by the Model Coupling Toolkit (MCT).

In the coupling region, the variables are exchanged between every domain of WRF and ROMS at a pre-set frequency, while in the non-coupling region the variables are changing according to their own model setting. In our study, SST is transmitted from ROMS to WRF, and wind stress, air temperature, air humidity, longwave radiation, shortwave radiation, latent heat flux, sensible heat flux, precipitation and evaporation are transmitted from WRF to ROMS every 60 seconds.

Figure 2 shows the models domain configuration of WRF and ROMS, respectively. The inner two domains of WRF is completely covered by the domain of ROMS. In the WRF model, three domains are adopted with the spatial resolution of 18km, 6km, and 2km, and the grid numbers of the domains are 311×251, 691×511, and 232×232, respectively. The innermost domain is vortex-following while the outer two are stationary. 50 vertical

sigma layers are adopted and the top layer in the model is 10hPa. Bogus is added by starting integration 24 hours ahead (Liu et al. [47]). The ROMS domain also has a 311×251 grid and a resolution of 18km as the outermost domain of WRF, and there are 40 vertical layers.

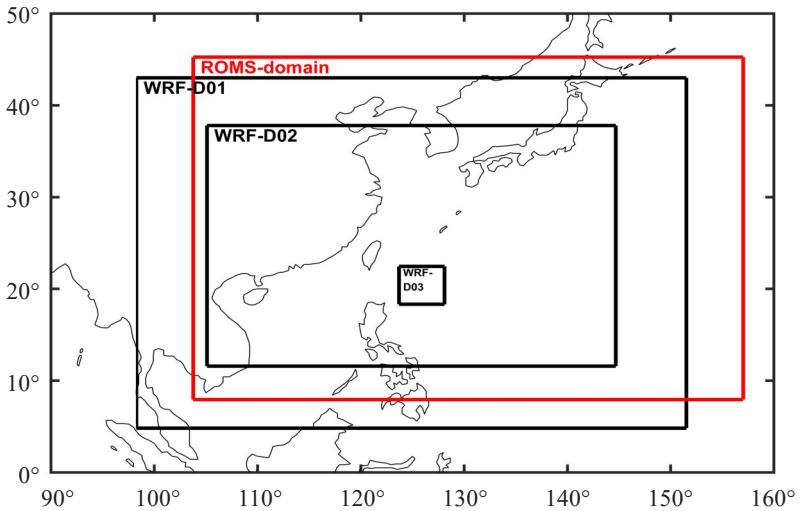

Figure 2. The model domains configuration.

Some primary parameterization schemes in the WRF are as follow: (1) New Thompson et al. microphysics scheme (Thompson et al. [48]), (2) Yonsei University planetary boundary layer scheme (Hong, Noh, and Dudhia [49]), (3) Kain-Fritsch cumulus parameterization (Kain and Fritsch [50]) (only activated in the outermost domain), (4) RRTM longwave radiation scheme (Mlawer et al. [51]) and Dudhia shortwave radiation scheme (Dudhia [52]). And some of the physical parameterization schemes choices in ROMS are: (1) *K*-profile vertical mixing parameterization, (2) Harmonic horizontal mixing parameterization, and (3) Splines density Jacobian for pressure gradient algorithm.

2.3 *Experimental design*

To investigate the specific influence of the warm water on the RI of Hato, two experiments were performed (see Table 1). The overarching issue of the experiments is to differentiate the contribution of the warm water while every other element is kept identical.

Table 1. Experimental design.

Experiment names	Models	Initial and boundary fields for ROMS	
		Surface	Subsurface
WARM	WRF-ROMS	SST on August 16, 2017	SODA data on August 16-21, 2017 average data, with warm water (real case)
CLIM	WRF-ROMS	SST on August 16, 2017	10-year-mean August climatological SODA data (from 2008 to 2017)

In exp. WARM, we wonder how Hato would develop with the existence of the warm water. That is to say, the atmospheric and oceanic environment where Hato is simulated should be as close to the real condition as possible. However,it is difficult to recognize the warm features in the input SODA data from August 16 to 21 mean, 2017, probably because of the rough 5-day temporal resolution, so it is necessary to adjust the temperature data. It has been found in early observation that all the meso-scale WCRs in oceans have highly similar structures and could be analyzed clearly (Zhang et al. [53]; Sun et al. [54]). Therefore, it is reasonable to reconstruct the temperature pattern of SODA data. The WCRs are reconstructed according to the one found in the South China Sea on July 24, 2010, which occurred in the same season and at a close location. In order to preserve the basic physical properties of the WCRs in the South China Sea, its average radial gradient of the temperature is reserved and the WCRs are reconstructed accordingly; similarly, the other warm water in the South China Sea is reconstructed according to the original water nearby. The temperature distribution of the second layer in SODA data (depth≈15m) before and after the warm water reconstruction is shown in Fig. 3. The dotted line box shows where the WCRs are reconstructed. In Fig. 3a, it can be seen that in the box, there is some positive anomaly of SST, which is a rough manifestation of the WCRs. However, they are not very clearly depicted, probably due to the coarse time resolution.

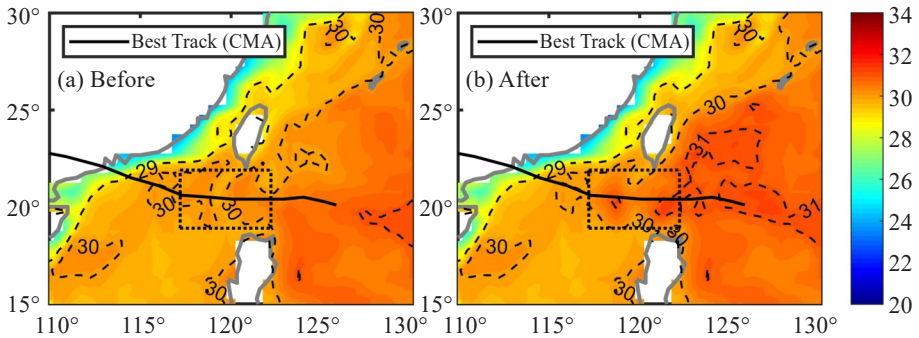

Figure 3. The distribution of temperature of the second layer (depth≈15m) of SODA data from August 16 to 21 mean before (a) and after (b) reconstruction in exp. WARM. The dashed line contours show the SST values and the dotted line rectangles show where the WCRs are reconstructed.

In exp. CLIM, the climatological data is used as the input. The climatological data is the 10-year-mean August climatological SODA data (from 2008 to 2017). It is worth mentioning that in both exp. WARM and exp. CLIM, only the subsurface data of the input SODA data differs, while the SST data of August 16, 2017 is reserved so that it can be seen that how SST changes with or without the subsurface warm water under the influence of Hato.

Each of the coupled simulations starts at 1800 UTC August 20, 2017 and operates for 90 hours. However, in order to make sure that ocean simulation remains stable, it is necessary to run ROMS separately ahead of time for 5 days or so before running the coupled model. This is also referred to as "spin-up". Therefore, the ROMS-only spin-up starts at 0000 UTC August 16. The stability of ROMS without external atmospheric forcing is also tested and it is found that ROMS could run stably for about 8 months. Therefore, in our study, the stability of simulation could be totally guaranteed.

3 RESULTS

3.1 *Observation*

According to the CMA best track data, Hato generated on 1800 UTC August 19 and made landfall at 0450 UTC August 23, 2017. From 0000 UTC 22 to 0000 UTC August 23, its MSLP deepened by 35hPa and its MSW increased by 20 m s^{-1} within 24 hours. Fig. 4 shows the variation of the MSLP and the MSW in 24 hours in the lifespan of Hato. According to previous studies and relevant standards (Shu et al. [55]), an RI process happens when the MSW increases by 15 m s^{-1} within 24 hours. It's obvious that Hato reached the grade at 0000 UTC August 23. Moreover, according to the statistical procedure, the average moving speed of Hato is around 24 km h^{-1}, which is faster than that in general cases. The translational speed of all the TCs in the Northwest Pacific Ocean in recent 10 years which acts in low-attitudes area (0° – 30° N) is no more than 18.5 km h^{-1}, according to Yang and Xia [56].

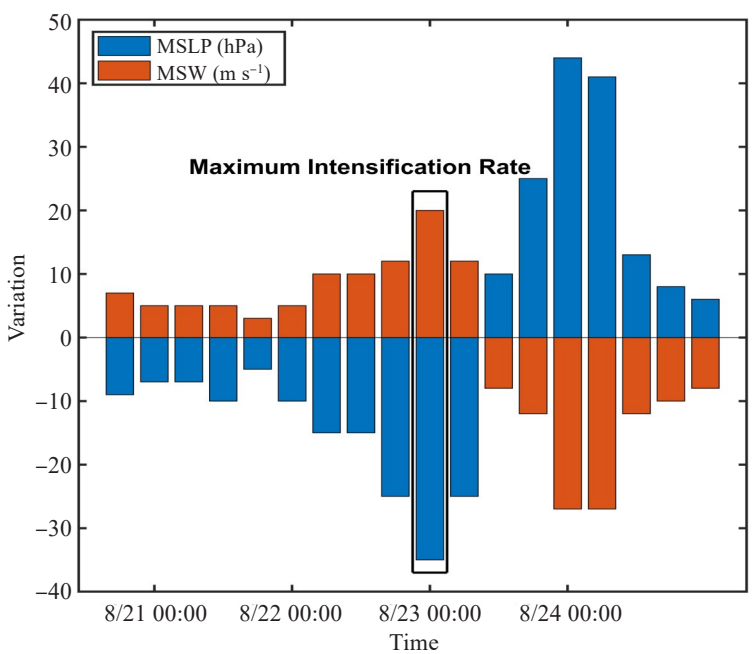

Figure 4. The variation of MSLP (blue bars, hPa) and MSW (red bars, m s^{-1}) within 24 hours according to the CMA best track.

Figure 1 shows the track of Hato and the distribution of SLA. The colorful dots on the tracks denote the intensity category classified by its MSW according to CMA standards, and the three big black circles highlight the warm water that Hato encountered, which existed right along the trajectory of Hato. The black arrows stand for the vertical wind shear of the environment field. As can be seen, Hato began to intensify rapidly after it encountered warm water. The vertical wind shear is the phasor difference between the wind vectors of 200hPa and 850hPa, and all of the grids whose distance to the center of Hato is more than 200km and less than 800km are included. The wind speed data is obtained from the FNL data. As a unit length equals 10 m s^{-1}, it is worth mentioning that the vertical wind shear along its trajectory is rather weak, which would also help the RI of Hato.

Figure 5 shows the daily SSTC distribution from August 20 to 23 compared with August 19, from OISST. It can be seen that the SSTC induced by Hato is quite weak. The maximum SSTC occurred on August 23 near the shore after Hato made landfall, which was no more than 3℃ . In the ocean, the SSTC is generally not stronger than 2℃.

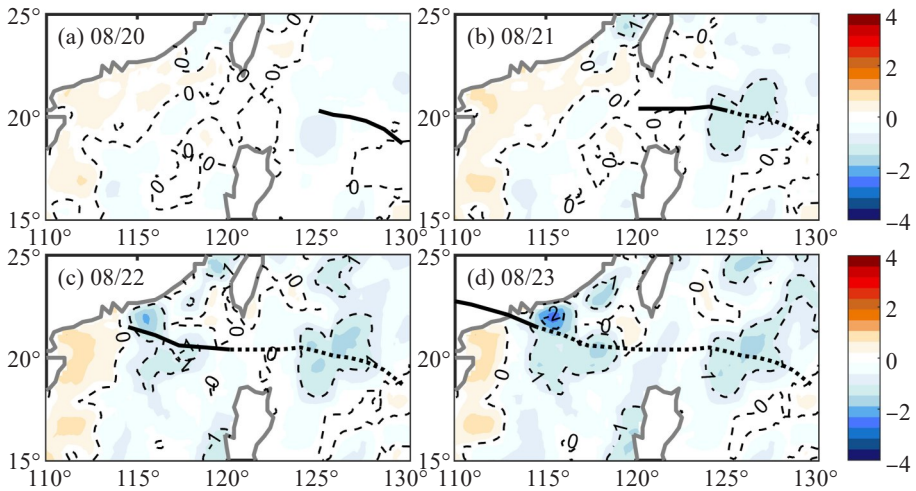

Figure 5. The SSTC distribution on August 20-23 compared with that on August 19 from OISST. Solid lines indicate the track of Hato on the particular day, and dotted lines indicate the track of Hato that it already passed. The dashed line contours show the SSTC values.

3.2 *Simulation results*

Correct analysis is based on correct data exchange between different models. The correctness is validated by comparing variables output from WRF and ROMS separately. It is verified that in the coupling region, those variables from different models are changing identically and synchronously, which means they are transferred properly; meanwhile, in the non-coupling region, the variables are changing respectively. In other words, in the non-coupling region, WRF and ROMS doesn't influence each other. The validation indicates that the coupled model is running correctly which means the consequences of simulations are credible and can be used for following analyses.

3.2.1 TRACK AND INTENSITY

Figure 6 shows the track results of the simulations of these two experiments, with the best track from CMA, JMA and JTWC. As can be seen, both experiments turn out to well simulate the track of Hato, with a slight time lag and southerly track error, which is acceptable.

Figure 7a and b respectively shows the MSW and the MSLP results of the simulations and the best track. The red shaded area stands for the period of time during which Hato interacts directly with the warm water features. Generally speaking, Hato goes through a similar RI trend in both two experiments. However, in the intensifying stage of Hato, the result of exp. WARM is basically identical to the best track data, while exp. CLIM obviously underestimates its intensity, especially the MSLP, which proves the rationality and the necessity of the warm water reconstruction. In its weakening stage, though exp. WARM is still basically stronger than exp. CLIM, they both overestimate intensity compared with the best track data. The common intensity overestimation in the later stage may be resulted from the time lag and the track error between the simulations and the observation; the time lag and the more south-easterly landing spot cause a longer time on the ocean. Therefore, Hato gained more energy from ocean and became stronger in intensity.

The composite reflectivity, which could represent the structure of TC, from observation, exp. WARM and exp. CLIM are shown in Fig. 8, at the time of landfall. It can be seen that they have a similar pattern, especially the convective rain band to the south of the eye, though the simulations are a little stronger. Despite the minor errors in the intensity, track and structure, these errors do not affect the analysis on the RI process of Hato.

Further analysis is taken on the intensity simulation

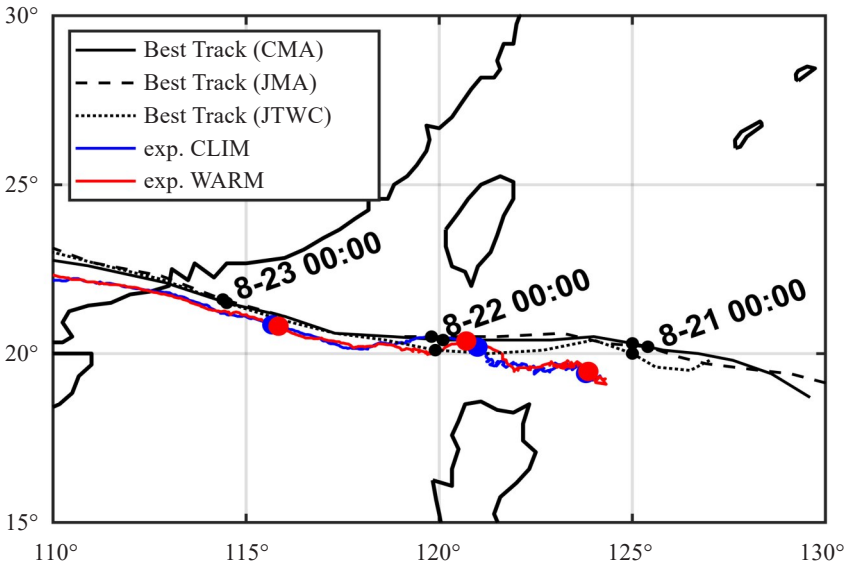

Figure 6. The track results of exp. WARM (red line) and exp. CLIM (blue line) and the best tracks.

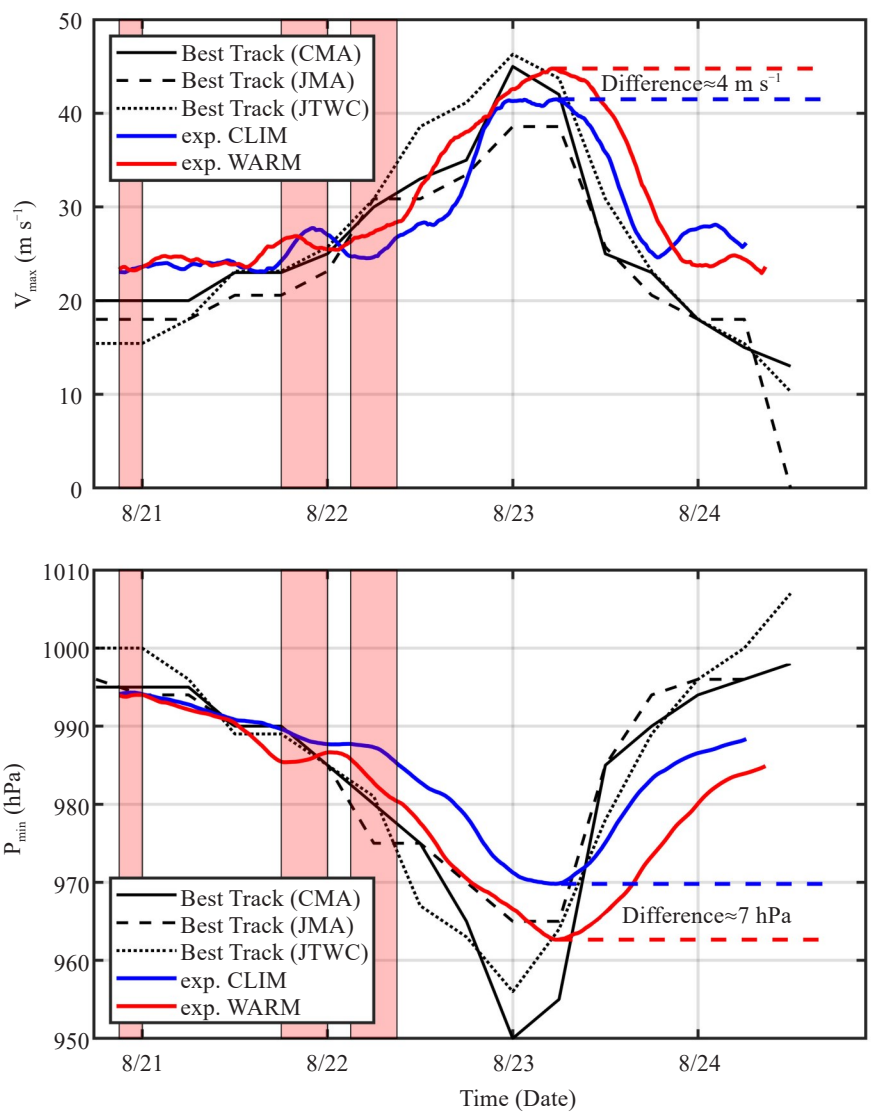

Figure 7. The intensity results of exp. WARM (red lines) and exp. CLIM (blue lines) and the best tracks. The red shaded area stands for the time when Hato interacts with the warm water features.

results. It is found that there is a 4m s^{-1} difference between the peak values of MSW and a 7hPa difference between the valley values of MSLP, which could take up around 20% of the intensification of Hato. According to Sun et al. [57], the impact ocean factors could impose on TC intensity is no more than 27% of the total intensification, which means the 20% difference in our study is reasonable and distinct.

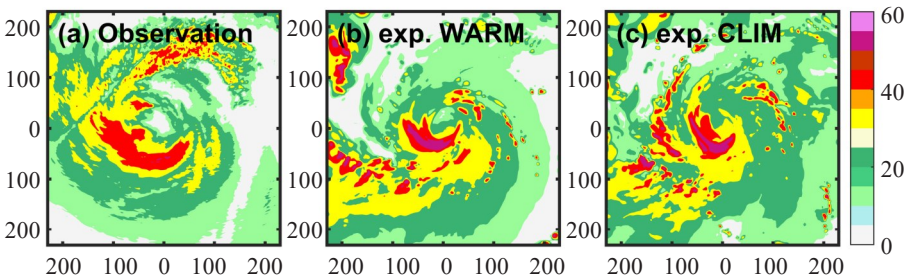

Figure 8. The composite reflectivity of Hato at the time of landfall from (a) observation from Guangzhou Radar Station, (b) exp. WARM and (c) exp. CLIM.

It is also noticed that the intensification rates in the two experiments are slightly different. Fig. 9 shows the 24-hour intensification rate in exp. CLIM (blue bars) and the difference between the two experiments (red bars stacked on blue bars, exp. WARM minus exp. CLIM), every 3 hours. Therefore, the total height stands for the 24-hour intensification rate in exp. WARM. Hato has a maximum intensification rate at 2100 UTC 22 in exp. WARM, while it is 0000 UTC 23 in exp. CLIM, which means Hato goes through an RI process in a very close period. Also, it can be seen there are 2 extremums, standing for the impact of the two WCRs. The first extremum occurred at 1200 UTC 22, and the second occurred at 2100 UTC August 22. According to the simulation results, Hato moved away from the first WCR at 0000 UTC 22, while it moved away from the other one at 0900 UTC 22 (Fig. 7), approximately. It can be concluded that the effect of warm water would totally come into play after 12 hours interacting with it.

These results clearly illustrate the role of the warm water; though it might not influence RI trend, it makes significant contribution to the RI process by around 20%.

3.2.2 SSTC

While the ocean beneath Hato is providing heat and moisture for Hato, SST is cooling accordingly. Fig. 10a, b and c show the SSTC pattern of the OISST, exp. WARM and exp. CLIM. According to OISST (Fig. 10a), the actual SSTC induced by Hato is quite weak. The average SSTC is roughly calculated by averaging the SSTC in the region where the SSTC is more than 0.5℃ in the activity sphere of Hato (110°–130°E, 18°–24°N). It turns out that the average SSTC induced by Hato is

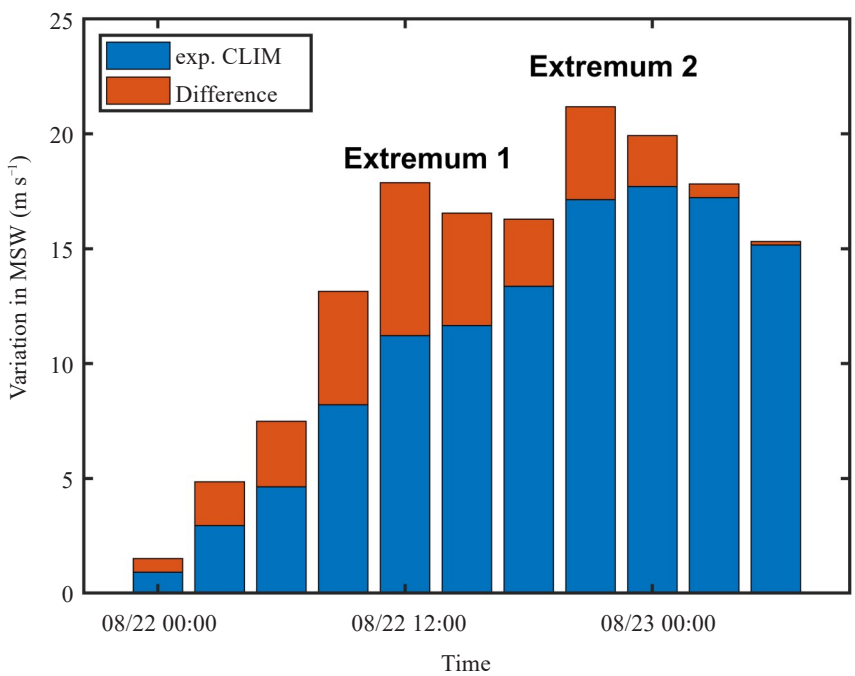

Figure 9. The 24-hour intensification rate in exp. CLIM (blue bars) and the difference between the two experiments (red bars, exp. WARM minus exp. CLIM).

around 0.73℃ , which is much weaker than that in general cases (Price [19]).

In exp. WARM (Fig. 10b), although in some particular area, like in the Luzon Strait and the nearshore region, the simulated SSTC is slightly stronger than the observed one, the SSTC results are generally very consistent with the observed SSTC results, both its pattern and intensity.

In exp. CLIM (Fig. 10c), what catches the attention most is it has a much wider and stronger SSTC outcome than that in exp. WARM, and also, observation. Before Hato comes into the South China Sea, intense SSTC occurs on the right side. As Hato is in Luzon Strait, the SSTC is also stronger, especially where the warm water should exist. When Hato comes into the South China Sea, stronger SSTC occurs again on the right side of the track, where the second WCR should be. It can be concluded that the much stronger SSTC can be attributed to the absence of the subsurface warm water to a great extent. In the real case, the warm water is the reason why the actual SSTC is weak.

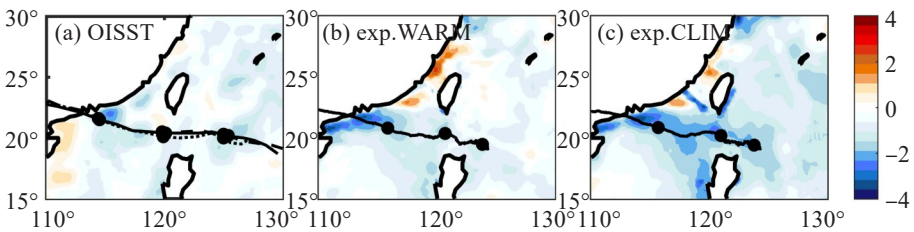

Figure 10. The distribution of SSTC induced by Hato and its track. (a) OISST and best track (solid line as CMA, dashed line as JMA and dotted line as JTWC), (b) exp. WARM, and (c) exp. CLIM. The three black dots on the tracks denote 0000 UTC 21, 22 and 23, August.

4 DISCUSSION

4.1 *Budget analysis of SSTC*

As mentioned above, there are two main mechanisms that could induce SSTC, i. e., vertical turbulent mixing and advection. That is, the vertical turbulent mixing of deep layer cold water and upper layer warm water caused by the vertical shear between ocean currents of different depth; the advection for the most part is the upwelling of deep-layer cold water caused by Ekman pumping. In ROMS, the sea water temperature is calculated according to Eq. (1):

$$\frac{\partial T}{\partial t} = -\vec{v}\cdot\nabla T - \frac{\partial}{\partial Z}\left(\overline{T'w'} - v_\theta\frac{\partial T}{\partial Z}\right) + F_T + D_T \quad (1)$$

This diagnostic equation clearly illustrates how temperature would change. In Eq. (1), $\frac{\partial T}{\partial t}$ is the local change; $-\vec{v}\cdot\nabla T$ is the horizontal advection; $-\frac{\partial}{\partial Z}\left(\overline{T'w'} - v_\theta\frac{\partial T}{\partial Z}\right)$ includes vertical advection and F_T and D_T stand for forcing terms and diffusive terms respectively. That is, if there is no external force, the advection (vertical plus horizontal) and the diffusion (namely vertical turbulent mixing) are the two main mechanisms for temperature change in ROMS. Fig. 11 shows the total SSTC, SSTC induced by vertical turbulent mixing and SSTC induced by advection in the two experiments, respectively. It turns out that, in both experiments, most of the SSTC near the trajectory of Hato is due to vertical turbulent mixing, while the effect of advection is negligible. In the nearshore region, there could even be SST warming caused by advection which could offset some SSTC produced by vertical turbulent mixing.

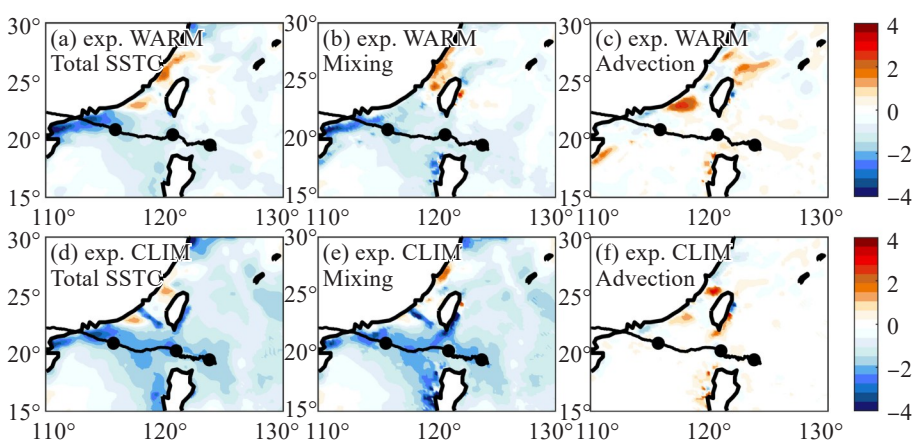

Figure 11. The distribution of (a) total SSTC, (b) SSTC due to mixing, and (c) SSTC due to advection in exp. WARM during the whole simulation and its simulated track. The three black dots on the tracks denote 0000 UTC 21, 22 and 23, August, and the black lines are the track result of the exp. WARM; (d)-(f) as in (a)-(c) but in exp. CLIM.

These phenomena could be ascribed to the presence of subsurface warm water. Where there is a warm water feature, there is a thicker local oceanic mixing layer, so the vertical turbulent mixing could not induce much SSTC. Besides, as can be seen that SSTC resulted from advection is quite weak in both experiments, probably because of the high translational speed of Hato. Therefore, it is mostly the warm water that caused the weak SSTC in the case.

4.2 *The thermal effects of different SSTC*

A host of previous studies point out that the heat and moisture flux on the interface of atmosphere and ocean is closely relevant to the SST; high SST would facilitate the heat and moisture transfer from ocean to atmosphere while the TC-induced SSTC could result in a decrease of the flux. In WRF model, the surface latent and sensible heat fluxes on the air-sea interface are calculated on the basis of the following bulk formulas, as shown in Eq. (2.1) and (2.2):

$$\mathrm{LH} = \rho L_v C_q U_a \left(q_g - q_a\right) \tag{2.1}$$

$$\mathrm{SH} = \rho c_p C_h U_a \left(T_g - T_a\right) \tag{2.2}$$

where LH and SH are short for latent heat flux and sensible heat flux. In Eq. (2.1), ρ is air density, L_v is the latent heat of vaporization, C_q is the exchange coefficient, U_a is wind speed, q is the water vapor mixing ratio, and $q_g - q_a$ stands for the water vapor difference value between air and sea. In Eq. (2.2), c_p is the heat capacity under specific pressure, C_h is the exchange coefficient, T is temperature and $T_g - T_a$ could represent the thermal difference between air and sea. Therefore, the higher the SST, the greater the thermal difference between ocean and atmosphere, and the better the heat and moisture transfer from sea to air.

In our study, the dependency of the structure of Hato and SST is also analyzed. Fig. 12 is the Hovmöller diagrams of different variables of Hato. The horizontal axis stands for radius and the vertical axis stands for time, and the black dashed lines stand for the time when Hato makes landfall. Therefore, the time variation trend of the variables that are azimuthally averaged could be clearly depicted. Fig. 12a and b shows the Hovmöller diagrams of the wind speed (shading, m s^{-1}) and the sea level pressure (isolines, hPa) of the two experiments, which is an intuitional expression of the TC structure and intensity. The maximum azimuthally wind speed could reach 35 m s^{-1} in exp. WARM while it is no more than 30 m s^{-1} in exp. CLIM. The minimum azimuthally sea level pressure is lower than 970hPa in exp. WARM while that of exp. CLIM is higher than 970hPa. It is pretty plain to see that exp. WARM has produced a more intense result.

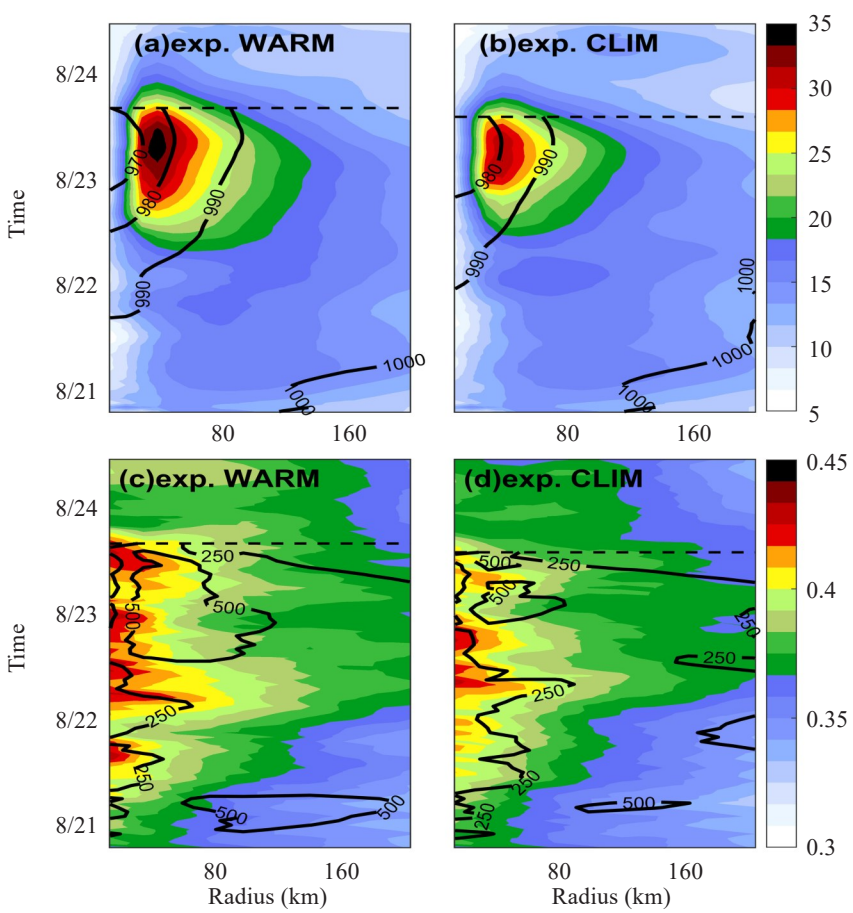

Figure 12. Hovmöller diagrams of the azimuthally average (a) wind speed (shading, m s^{-1}) and sea level pressure (isolines, hPa), (c) water vapor mixing ratio (shading, kg kg^{-1}) and heat flux (isolines, W m^{-2}). (b) and (d) as in (a), (c) but in exp. CLIM. The black dashed lines stand for the time when Hato makes landfall.

Figure 12c and d show the Hovmöller diagrams of the total water vapor mixing ratio (shading, kg kg^{-1}) in a vertical column and the heat flux (isolines, W m^{-2}) on the interface. The heat flux being positive means it goes from the ocean to the air. As can be seen, in exp. WARM, the heat flux is obviously stronger than that in exp. CLIM; also, in the inner part of Hato (within 100km), the moisture content in exp. WARM is always more than that in exp. CLIM. Moreover, the high value zones of the variables are overlapping to some extent, which is revealing their dependency on each other.

To quantify the thermal effects of the warm water, the average latent, sensible and total heat flux during the RI (from 0000 UTC 22 to 0000 UTC 23) within 160 km are calculated and compared (see Table 2). In exp. WARM, the average latent, sensible, total heat flux is 371.2 W m^{-2}, 49.3 W m^{-2} and 420.5 W m^{-2} respectively. Meanwhile in exp. CLIM, the values are 301.1 W m^{-2} 39.2 W m^{-2}, and 340.3 W m^{-2}. It can be further calculated that the latent, sensible, and total heat flux in exp. WARM are more than those of exp. CLIM by 18.9%, 20.5%, 19.1%, which is exactly the thermal effect of the warm water. It can be concluded that the warm water provides more heat for Hato by about 20%, which matches the intensity difference mentioned in section 3.2.1.

Table 2. Mean heat fluxes from 0000 UTC 22 to 0000 UTC 23 August within 160 km around center of Hato.

	Latent heat flux	Sensible heat flux	Total heat flux
Exp. WARM	371.2 W m^{-2}	49.3 W m^{-2}	420.5 W m^{-2}
Exp. CLIM	301.1 W m^{-2}	39.2 W m^{-2}	340.3 W m^{-2}
Difference	70.1 W m^{-2}	10.1 W m^{-2}	80.2 W m^{-2}
Portion	18.9%	20.5%	19.1%

Figure 13 shows the radar composite reflectivity factor at 3 km height of three moments during the RI process in the two experiments. Radar reflectivity factor (dBZ) represents the content of water of all phases, like raindrops, cloud water, water vapor and solid particles like ice and snow, which is often used to describe the TC structure. In exp. WARM, as can be seen, the structure of Hato is much more compact and organized, while it is more scattered in exp. CLIM.

Now it is known that in the case of Hato, SST influences the structure of Hato in a profound way, like many researchers found before. The study of Jiang et al. has verified the strong correlation of the heat flux and the SST beneath the TC: the TC-induced SSTC not only decreases the latent heat flux, but also turns the sensible heat flux downward in their case [58]. That happens when TC induces strong SSTC: when SST is even cooler than the atmosphere, the sensible heat goes from the air to the ocean. Meanwhile, the SSTC reacts upon the TC, resulting in a more asymmetric structure especially in the middle and high level. Moreover, Lei put forward that the diabatic heating could cause significant asymmetry on the radial inhomogeneity structure of TC wind [59]. Their studies lay the groundwork for us and future research.

As a matter of fact, the physical nature of the warm water influencing the intensity of Hato also lies in there. Emanuel put forward the famous wind-induced surface heat exchange (known as WISHE mechanism), shedding light on the important role the heat flux plays in the intensification of TC [8]. The essence of WISHE mechanism is the positive feedback between the heat flux and flow field. With the heat flux going into the TC, the TC intensifies and the wind field at the bottom layer gets stronger, which could in turn reinforces the heat flux, as is shown in equation (2.1) and (2.2). Such a feedback is of great significance to the TC development, and also applies for our study. Although there might be some controversies and criticisms on the theory (e. g., Montgomery et al. [60]), there is indeed a strong dependence between SST and heat and moisture flux, and it is true that they are important for the development of a TC.

In conclusion, in this case, due to the warm water and the fast movement speed of Hato, the SSTC induced by Hato is not so strong as other cases, which means its inhibiting effect is restrained. Therefore, the heat and moisture flux aren't impaired much but being provided sufficiently on the contrary. As a result, the structure of Hato is more compact and hence the stronger intensity.

Till now, it can be certainly concluded that the warm water features are truly essential for the development of Hato. Analogical research have similar conclusions that could support ours. The studies of Hong et al. [35] and Shay et al. [36] both verified the importance of the WCR to Opal (1995); Wang et al. [40] also confirmed that without interacting with the WCR, typhoon Haiyan wouldn't be as strong as it is.

It should be remembered that the RI of Hato is a complex result of a variety of reasons. In fact, the appropriate atmospheric condition is also very important for RI of TCs (Zhang et al. [61]; Yu et al. [62]). As mentioned in previous studies (Zhang et al. [41]; Qin et al. [42]), the weak vertical wind shear, the favorable

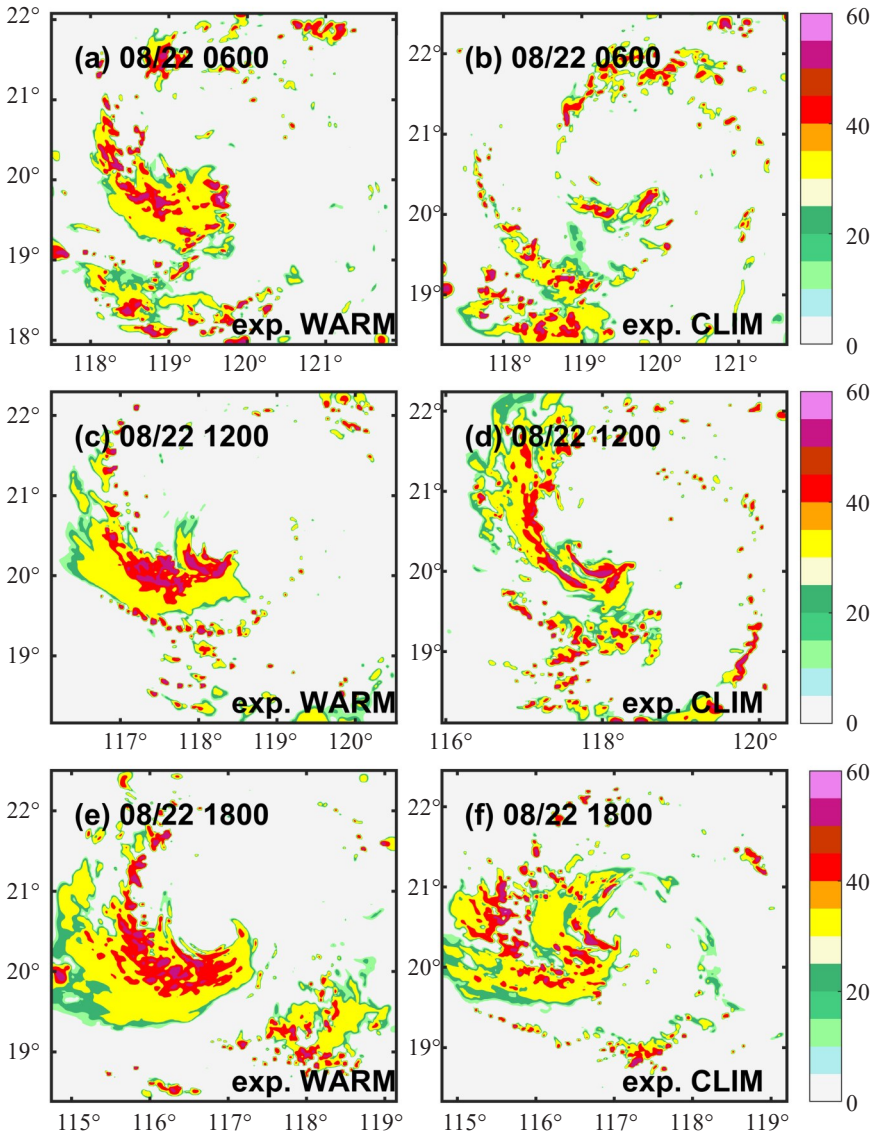

Figure 13. Radar reflectivity factor (dBZ) at 3-km height on (a) 08/22 0600, (c) 08/22 1200, and (e) 08/22 1800 in exp. WARM. (b), (d), (f) as in (a), (c), (e) but in exp. CLIM.

environment flow field and the abundant moisture all contributed. More work should be done if we want to thoroughly understand the mechanism of the RI process of Hato.

5 CONCLUSION

Typhoon Hato generated in the northwestern Pacific on August 20, 2017 and made landfall in Zhuhai, Guangdong Province at 0450 UTC on August 23, 2017. It has attracted broad attention because of its destructive power. According to the CMA best track data, Hato went through a RI process; within 24 hours, its MSLP deepened by 35hPa and its MSW increased by 20 m s^{-1}. Besides, according to satellite altimeter data, before going through the RI process, Hato moved over a large area of warm water to the east of Luzon Strait, and then two WCRs in the South China Sea along its trajectory moved on the ocean. Although it is known to all that TC may cause SSTC, OISST data shows that the average SSTC induced by Hato is only about 0.73 ℃, which is not so strong as that in other TC cases.

A lot of previous studies confirm that ocean plays a key role in the development of TC; there are both positive and negative feedback between them. On one hand, ocean provides heat and moisture for TC intensification; on the other hand, SSTC induced by TC could restrain energy transfer and hold back its development. Besides, the meso-scale features in the ocean may influence TCs by changing local ocean subsurface condition. Thus, it is reasonable to assume that warm water has great impact on RI process. Air-sea coupled models are used to carry out numerical simulations to analyze the magnitude of their contribution and corresponding mechanism.

COAWST model is the main instrument and its WRF and ROMS components are used in the current

research. To figure out the role of the warm water, two experiments have been implemented, i. e., exp. WARM and exp. CLIM. In exp. WARM, after reconstructing the temperature pattern, the oceanic environment is significantly more similar to the observation so the case is run with the warm water features taken into account. In exp. CLIM, climatological data is input to make sure the warm water features no longer exist.

Consequences of the two experiments are compared. Both of them have good tracks consequences with a slight time lag. As for intensity, the simulation results indicate that although Hato would go through the RI process with or without the warm water, the warm water has a significant influence on it. Around 20% of the total RI is contributed by the warm water, and the effect of the warm water would arise after 12-hours interaction with them. SST underneath Hato is also changing accordingly. Exp. WARM has a better SSTC simulation consequence while in exp. CLIM SSTC occurs more widely and strongly.

Further analysis is taken on the SSTC budget. It is found that the SSTC is mostly triggered by vertical turbulent mixing. On one hand, the warm water deepens the local oceanic mixing layer so the vertical turbulent mixing could not induce much SSTC; on the other hand, the cold advection takes up a very small part in the SSTC in both experiments, which might be due to the high translational speed of Hato. Our study verifies that the weak SSTC induced by Hato is largely resulted from the warm water so that the negative feedback is also restrained.

SST is an essential factor for the heat and moisture exchange between the atmosphere and ocean. High SST would help more heat transfer from ocean to atmosphere. In exp. WARM, during the RI of Hato, plenty of heat and moisture has been transferred from the ocean to Hato. As a result, the distribution of water vapor and heat flux in the inner region of Hato all varies with time between two experiments following a regular pattern. The warm water helps heat flux increase by around 20%. According to the 3km height radar reflectivity, Hato has a more compact and organized structure in exp. WARM, which could be attributed to the weak SSTC caused by the warm water. It can be concluded that the warm water has a great impact on the structure of Hato and eventually facilitates the RI process.

Although the warm water does not completely account for the RI process, it is a very indicative factor for the TC intensity forecast anyway. More work is needed to unveil the thorough mechanism of the RI of Hato.

REFERENCES

[1] WANG Qian, QIAN Chuan-hai, ZHANG Ling. The characteristics and impact of typhoon activities over western North Pacific and the South China Sea [J]. J Marine Meteorol, 2018, 38(2): 1-11 (in Chinese).

[2] ELSBERRY R L, HOLLAND G J, GERRISH H, et al. Is there any hope for tropical cyclone intensity prediction? — a panel discussion [J]. Bull Amer Meteorol Soc, 1992, 73 (3): 264-275, https://doi.org/10.1175/1520-0477-73.3.264.

[3] MERRILL R T. Environmental influences on hurricane intensification [J]. J Atmos Sci, 1988, 45(11): 1678-1687, https://doi.org/10.1175/1520-0469(1988)045<1678:EIOHI>2.0.CO;2.

[4] EMANUEL K A. Thermodynamic control of hurricane intensity [J]. Nature, 1999, 401(6754): 665-669, https://doi.org/10.1038/44326.

[5] KAPLAN J, DeMARIA M. Large-scale characteristics of rapidly intensifying tropical cyclones in the North Atlantic Basin [J]. Wea Forecasting, 2003, 18(6): 1093-1108, https://doi.org/10.1175/1520-0434(2003)018<1093:LCORIT>2.0.CO;2.

[6] WANG Yu-qing, WU Chun-chieh. Current understanding of tropical cyclone structure and intensity changes - a review [J]. Meteor Atmos Phys, 2004, 87(4): 257-278, https://doi.org/10.1007/s00703-003-0055-6.

[7] DUAN Yi-hong, YU Hui, WU Rong-sheng. Review of the research in the intensity change of tropical cyclone [J]. Acta Meteor Sinica, 2005, 63(5): 636-645 (in Chinese).

[8] EMANUEL K A. An air-sea interaction theory for tropical cyclones, Part I: steady-state maintenance [J]. J Atmos Sci, 1986, 43(6): 585-605, https://doi.org/10.1175/1520-0469(1986)043<0585:AASITF>2.0.CO;2.

[9] PALMÉN E. On the formation and structure of tropical hurricanes [J]. Geophysica, 1948, 3: 26-38.

[10] MILLER B I. On the maximum intensity of hurricanes [J]. J Meteor, 1958, 15: 184-195.

[11] EMANUEL K A. The maximum intensity of hurricanes [J]. J Atmos Sci, 1988, 45(7): 1143-1155.

[12] XU Jing, WANG Yu-qing, TAN Zhe-min. The relationship between sea surface temperature and maximum intensification rate of tropical cyclones in the North Atlantic [J]. J Atmos Sci, 2016, 73(12): 4979-4988, https://doi.org/10.1175/JAS-D-16-0164.1.

[13] CIONE J J, UHLHORN E W. Sea surface temperature variability in hurricanes: implications with respect to intensity change [J]. Mon Wea Rev, 2003, 131(8): 1783-1796, https://doi.org/10.1175//2562.1.

[14] ZHENG Feng, YUE Cai-jun, CHEN Pei-yan, et al. Effects of SST, VWS, and DCC upon rapid intensification of offshore typhoons in China seas [J]. J Trop Meteor, 2019, 25 (1): 11-23, https://doi. org / 10.16555 / j. 1006-8775.2019.01.002.

[15] WANG Qin, LI Shuang-lin, FU Jian-jian. The influences of SSTA over Kuroshio and its extension on rainfall in northeast China under the background of two different El Niño cases [J]. J Trop Meteor, 2018, 24(2): 232-242, https://doi.org/10.16555/j.1006-8775.2018.02.011.

[16] WANG Wei, WANG Yan, QU Ping, et al. Diurnal variation of SST in relation to season and weather phenomena in the Bohai region [J]. J Trop Meteor, 2019, 25(3): 399-413, https://doi. org / 10.16555 / j. 1006-8775.2019.03.011.

[17] CHANG S W, ANTHES R A. The mutual response of the tropical cyclone and the ocean [J]. J Phys Oceanogr, 1979, 9: 128-135.

[18] LEIPPER D F. Observed ocean conditions and Hurricane

Hilda [J]. J Atmos Sci, 1964, 24(2): 182-186.
[19] PRICE J F. Upper ocean response to a hurricane [J]. J Phys Oceanogr, 1981, 11(2): 153-175.
[20] CHU P C, VENEZIANO J M, FAN Chen-wu, et al. Response of the South China Sea to Tropical Cyclone Ernie 1996 [J]. J Geophys Res Ocean, 2000, 105(C6): 13991-14009, https://doi.org/10.1029/2000jc900035.
[21] JACOB S D, SHAY L K, MARIANO A J, et al. The 3D oceanic mixed layer response to Hurricane Gilbert [J]. J Phys Oceanogr, 2000, 30(6): 1407-1429, https://doi.org/10.1175/1520-0485(2000)0302.0.CO;2.
[22] LIN I I, LIU W T, WU Chun-chieh, et al. Satellite observations of modulation of surface winds by typhoon-induced upper ocean cooling [J]. Geophys Res Lett, 2003, 30(3): 311-314, https://doi.org/10.1029/2002GL015674.
[23] SANFORD T B, PRICE J F, GIRTON J B. Upper-ocean response to Hurricane Frances (2004) observed by profiling EM-APEX floats [J]. J Phys Oceanogr, 2011, 41 (6): 1041-1056, https://doi.org/10.1175/2010JPO4313.1.
[24] POTTER H, DRENNAN W M, GRABER H C. Upper ocean cooling and air-sea fluxes under typhoons: A case study [J]. J Geophys Res Ocean, 2017, 122(9): 7237-7252, https://doi.org/10.1002/2017JC012954.
[25] GINIS I. Tropical cyclone-ocean interactions [J]. Advances in Fluid Mechanics, 2002, 33: 83-114.
[26] SCHADE L R, EMANUEL K A. The ocean's effect on the intensity of tropical cyclones: results from a simple coupled atmosphere-ocean model [J]. J Atmos Sci, 1999, 56(4): 642-651, https://doi.org/10.1175/1520-0469(1999)056<0642:TOSEOT>2.0.CO;2.
[27] CHAN J C L, DUAN Yi-hong, SHAY L K. Tropical cyclone intensity change from a simple ocean-atmosphere coupled model [J]. J Atmos Sci, 2001, 58(2): 154-172, https://doi. org / 10.1175 / 1520-0469(2001)058<0154:TCICFA>2.0.CO;2.
[28] DAVIS C, WANG Wei, CHEN S S, et al. Prediction of landfalling hurricanes with the advanced hurricane WRF model [J]. Mon Wea Rev, 2008, 136(6): 1990-2005, https://doi.org/10.1175/2007MWR2085.1.
[29] ZENG Zhi-hua, CHEN Lian-shou. Numerical experiments of the effect of oceanic mixing layer depth on TC structure and intensity changes [J]. Plateau Meteorology, 2011, 30(6): 1584-1593 (in Chinese).
[30] DUAN Yi-hong, WU Rong-sheng, YU Run-ling, et al. Numerical simulation of changes in tropical cyclone intensity using a coupled air-sea model [J]. Acta Meteor Sinica, 2013, 27(5): 658-672, https://doi. org / 10.1007 / s13351-013-0503-2.
[31] LI Chan-zhu, YANG Song, LI Chun-hui, et al. Seasonal predictions for spring and autumn surface air temperatures over southern China by the NCEP CFSv2 [J]. J Trop Meteor, 2019, 25(4): 448-461, https://doi.org/10.16555/j.1006-8775.2019.04.003.
[32] ZHAO Xiao-hui, CHAN J C L. Changes in tropical cyclone intensity with translation speed and mixed-layer depth: idealized WRF-ROMS coupled model simulations [J]. Q J R Meteorol Soc, 2017, 143(702): 152-163, https://doi.org/10.1002/qj.2905.
[33] LIU Xin, WEI Jun, ZHANG Da-lin, et al. Parameterizing sea surface temperature cooling induced by tropical cyclones, 1: theory and an application to Typhoon Matsa (2005) [J]. J Geophys Res Oceans, 2019, 124(2): 1215-1231, https://doi.org/10.1029/2018JC014117.
[34] LIU Xin, ZHANG Da-lin, GUAN Jian. Parameterizing sea surface temperature cooling induced by tropical cyclones, 2: verification by ocean drifters [J]. J Geophys Res Oceans, 2019, 124(2): 1232-1243, https://doi. org / 10.1029/2018JC014118.
[35] HONG Xiao-dong, CHANG S W, RAMAN S, et al. The interaction between Hurricane Opal (1995) and a warm core ring in the Gulf of Mexico [J]. Mon Wea Rev, 2000, 128(5): 1347-1365, https://doi. org / 10.1175 / 1520-0493(2000)128<1347:TIBHOA>2.0.CO;2.
[36] SHAY L K, GONI G J, BLACK P G. Effects of a warm oceanic feature on Hurricane Opal [J]. Mon Wea Rev, 2000, 128(5): 1366-138, https://doi. org / 10.1175 / 1520-0493(2000)128<1366:EOAWOF>2.0.CO;2.
[37] LIN I I, WU Chun-chieh, EMANUEL K A, et al. The interaction of Super-typhoon Maemi (2003) with a warm ocean eddy [J]. Mon Wea Rev, 2005, 133(9): 2635-2649, https://doi.org/10.1175/MWR3005.1.
[38] LIN I I, WU Chun-chieh, PUN Iam-fei, et al. Upper-ocean thermal structure and the western north pacific category 5 typhoons, Part I: ocean features and the category 5 typhoons' intensification [J]. Mon Wea Rev, 2008, 136 (9): 3288-3306, https://doi.org/10.1175/2008MWR2277.1.
[39] KUO Yi-chun, ZHENG Zhe-wen, ZHENG Quan-an, et al. Typhoon Kuroshio interaction in an air-sea coupled system: Case study of Typhoon Nanmadol (2011) [J]. Ocean Model, 2018, 132: 130-138, https://doi. org / 10.1016/j.ocemod.2018.10.007.
[40] WANG Guan-suo, ZHAO Biao, QIAO Fang-li, et al. Rapid intensification of Super Typhoon Haiyan: the important role of a warm-core ocean eddy [J]. Ocean Dyn, 2018, 68(12): 1649-1661, https://doi. org / 10.1007 / s10236-018-1217-x.
[41] ZHANG Jing, SHI Da-wei, LI Chao. Analysis on the sudden change and its cause of Typhoon Hato [J]. Marine Forecasts, 2018, 35(2): 36-43 (in Chinese).
[42] QIN Li, WU Qi-shu, ZENG Xiao-tuan, et al. Analysis on cause of rapid intensification of asymmetrical Typhoon Hato (1713) over the offshore of China [J]. Torrential Rain and Disasters, 2019, 38(3): 212-220 (in Chinese).
[43] YING Ming, ZHANG Wei, YU Hui, et al. An overview of the China meteorological administration tropical cyclone database [J]. J Atmos Ocean Tech, 2014, 31(2): 287-301, https://doi.org/10.1175/JTECH-D-12-00119.1.
[44] CARTON J A, CHEPURIN G, CAO Xian-he, et al. A simple ocean data assimilation analysis of the global upper ocean 1950–95, Part 1: methodology [J]. J Phys Oceanogr, 2000, 30(2): 294-309, https://doi.org/10.1175/1520-0485(2000)030<0294:ASODAA>2.0.CO;2.
[45] CARTON J A, CHEPURIN G, CAO Xian-he. A simple ocean data assimilation analysis of the global upper ocean 1950–95, Part 2: results [J]. J Phys Oceanogr, 2000b, 30 (2): 311-326, https://doi.org/10.1175/1520-0485(2000)030<0311:ASODAA>2.0.CO;2.
[46] WARNER J C, ARMSTRONG B, HE R, et al. Development of a Coupled Ocean-Atmosphere-Wave-Sediment Transport (COAWST) modeling system [J]. Ocean Modelling, 2010, 35(3): 230-244, https://doi.org/10.1016/j.ocemod.2010.07.010.
[47] LIU Hao-yan, WANG Yu-qing, XU Jing, et al. A dynamical initialization scheme for tropical cyclones

under the influence of terrain [J]. Wea forecasting, 2018, 33(3): 641-659, https://doi. org / 10.1175 / WAF-D-17-0139.1.

[48] THOMPSON G, FIELD P R, RASMUSSEN R M, et al. Explicit forecasts of winter precipitation using an improved bulk microphysics scheme, part ii: implementation of a new snow parameterization [J]. Mon Wea Rev, 2008, 36(12): 5095-5115, https://doi. org / 10.1175/2008MWR2387.1.

[49] HONG Song-you, NOH Y, DUDHIA J. A new vertical diffusion package with an explicit treatment of entrainment processes [J]. Mon Wea Rev, 2006, 134(9): 2318-2341, https://doi.org/10.1175/MWR3199.1.

[50] KAIN J S, FRITSCH J M. A one-dimensional entraining/detraining plume model and its application in convective parameterization [J]. J Atmos Sci, 1990, 47(23): 2784-2802, https://doi.org/10.1175/1520-0469(1990)047<2784:AODEPM>2.0.CO;2.

[51] MLAWER E J, TAUBMAN S J, BROWN P D, et al. Radiative transfer for inhomogeneous atmospheres: RRTM, a validated correlated-k model for the longwave [J]. J Geophys Res Atmos, 1997, 102(D14): 16663-16682, https://doi.org/10.1029/97JD00237.

[52] DUDHIA J. Numerical study of convection observed during the winter monsoon experiment using a mesoscale two-dimensional model [J]. J Atmos Sci, 1989, 46(20): 3077-3107, https://doi.org/10.1175/1520-0469(1989)046<3077:NSOCOD>2.0.CO;2.

[53] ZHANG Zheng-guang, WANG Wei, QIU Bo. Oceanic mass transport by mesoscale eddies [J]. Science, 2014, 345(6194): 322-324, https://doi. org / 10.1126 / science.1252418.

[54] SUN Wen-jin, DONG Chang-ming, WANG Ru-yun, et al. Vertical structure anomalies of oceanic eddies in the Kuroshio Extension region [J]. J Geophys Res Oceans, 2017, 122(2): 1476-1496, https://doi. org / 10.1002 / 2016JC012226.

[55] SHU Shou-juan, MING Jie, CHI Peng. Large-scale characteristics and probability of rapidly intensifying tropical cyclones in the western North Pacific Basin [J]. Wea Forecasting, 2012, 27(2): 411-423, https://doi. org / 10.1175/WAF-D-11-00042.1.

[56] YANG Ya-xin, XIA Jian-dong. Characteristics of Northwest Pacific tropical cyclones [J]. Navigation of China, 2019, 42(2): 114-119 (in Chinese).

[57] SUN J, OEY L, XU F, et al. Sea level rise, surface warming, and the weakened buffering ability of South China Sea to strong typhoons in recent decades [J]. Scientific Reports, 2017, 7(1), https://doi. org / 10.1038 / s41598-017-07572-3.

[58] JIANG Xiao-ping, LIU Chun-xia, MO Hai-tao, et al. The impact of air-sea interactions on typhoon structure [J]. J Trop Meteor, 2010, 26(1): 55-59 (in Chinese).

[59] LEI Xiao-tu. The influence of diabatic heating on tropical cyclone radial inhomogeneity structure [J]. Acta Ocean Sinica, 2000, 22(04): 24-30 (in Chinese).

[60] MONTGOMERY M T, SANG N V, SMITH R K, et al. Do tropical cyclones intensify by WISHE? [J]. Q J R Meteorol Soc, 2009, 135(644): 1697-1714, https://doi.org/10.1002/qj.459.

[61] ZHANG Sheng-jun, QIAN Yan-zhen, HUANG Yi-wu, et al. Numerical simulation study on the rapid intensification of Typhoon Haikui (1211) off the shore of China [J]. J Trop Meteor, 2017, 23(3): 269-280, https://doi.org/10.16555/j.1006-8775.2017.03.004.

[62] YU Xin, ZHENG Teng-fei, WAN Qi-lin, et al. Causal analysis and numerical modeling of the inshore intensification of super typhoon "Hato" [J]. J Trop Meteor, 2019, 25(3): 292-303, https://doi. org / 10.16555 / j.1006-8775.2019.03.001.

Citation: HUO Zi-mo, DUAN Yi-hong, and LIU Xin. The effect of the warm water and its weak negative feedback on the rapid intensification of Typhoon Hato (2017) [J]. J Trop Meteor, 2020, 26(4): 402-416, https://doi.org/10.46267/j.1006-8775.2020.035.